

Physics-Based and Closed-Form Model for Cryo-CMOS Subthreshold Swing

Arnout Beckers , Jakob Michl , Alexander Grill , Ben Kaczer , Marie Garcia Bardon , Bertrand Parvais , Bogdan Govoreanu , Kristiaan De Greve , Gaspard Hiblot  and Geert Hellings 

Abstract—Cryogenic semiconductor device models are essential in designing control systems for quantum devices and in benchmarking the benefits of cryogenic cooling for high-performance computing. In particular, the saturation of subthreshold swing due to band tails is an important phenomenon to include in low-temperature analytical MOSFET models as it predicts theoretical lower bounds on the leakage power and supply voltage in tailored cryogenic CMOS technologies with tuned threshold voltages. Previous physics-based modeling required to evaluate functions with no closed-form solutions, defeating the purpose of fast and efficient model evaluation. Thus far, only the empirically proposed expressions are in closed form. This article bridges this gap by deriving a physics-based and closed-form model for the full saturating trend of the subthreshold swing from room down to low temperature. The proposed model is compared against experimental data taken on some long and short devices from a commercial 28-nm bulk CMOS technology down to 4.2 K.

Index Terms—Band Tail, Cryogenic, MOSFET

I. INTRODUCTION

IN recent years, cryo-CMOS has emerged as the leading candidate for controlling quantum devices due to its proven performance down to deep-cryogenic temperatures and its potential for monolithic integration with quantum bits [1]–[3]. Other cutting-edge physics experiments, like gravitational wave or dark matter detection, can also benefit from the increased attention for cryo-CMOS devices and circuits [4], [5]. Furthermore, datacenters could benefit from advanced CMOS technologies tailored to cryogenic operation [6], [7].

Steepness of the transistor switching between ON- and OFF-states at cryogenic temperatures is an essential performance metric for the aforementioned applications. In a MOSFET, the inverse slope of the subthreshold current in \log_{10} -scale, a.k.a. subthreshold swing, SS , is expected to scale linearly with temperature (T), following Boltzmann’s thermal limit,

$$SS_{(T \gg T_c)} = m \cdot \frac{k_B T}{q} \cdot \ln(10), \quad (1)$$

where m is the subthreshold-slope factor, k_B is Boltzmann’s constant, and q is the electron charge.

However, SS deviates from this linear scaling around a certain critical temperature, T_c , typically around 50 K. In previous literature [8]–[10], SS has been shown to saturate to a temperature-independent plateau below T_c ,

$$SS_{(T \ll T_c)} = m \cdot \frac{k_B T_c}{q} \cdot \ln(10), \quad (2)$$

The authors are with imec, Leuven, Belgium (arnout.beckers@imec.be). B. Parvais is also with the Vrije Universiteit Brussel, Belgium. K. De Greve is also with KU Leuven. J. Michl was with the Institute for Microelectronics, TU Vienna, Austria, at the time of initial submission.

where T_c links to the characteristic exponential decay of a band tail, i.e., $W_{t,c} = k_B T_c$. Such band tails have already been demonstrated experimentally using electron-spin resonance in silicon MOS devices at 370 mK [11]. Interface and source/drain engineering give SS closer to the thermal limit [12], [13]. Besides band tails, direct source-to-drain tunneling is an additional explanation for saturation of SS at cryogenic temperatures in short devices [14], [15].

Limits (1) and (2) are physics-based models, but they cover only part of the T -domain. To capture the full saturating trend across T_c , different models are being used. The physics-based models numerically integrate the Fermi-Dirac integrals with exponential density-of-states [8], [10], or use Gauss hypergeometric functions [9], which are not of closed form and thus difficult to implement in compact models. On the other hand, suitable curve fits are available connecting the two limits, e.g., $\propto \ln(1 + e^x)$ [(7), [10]] or $\propto \sqrt{1 + x^2}$ [(9), [16]].

From (1) and (2) it is clear that a T_c/T -dependence must appear out of the physics derivation to complete the transition below T_c in a full T -range model. Such a $\propto 1/T$ -dependence has been postulated since 1985 [17] but is nowadays often inserted empirically in the Boltzmann limit with the help of an effective slope factor [18], [19] or an effective temperature [16]. It has not been derived in a physical model thus far. The closest attempt were the discrete trap states close to the band edge in [20] which gave a $\propto 1/T$ -dependence at the state energy. This $\propto 1/T$ must also follow from a physics-based derivation for a continuous tail of states close to the band edge. In this article, such a T_c/T -dependence is derived inside a physics-based and closed-form model for SS covering the whole temperature domain from ≈ 0 K to 300 K (Section II). We explore the sensitivity of the physical model parameters and compare the model with experimental data (Section III).

II. MODEL DERIVATION & DISCUSSION

A. Exponential Band Tail

Fig. 1 clarifies, from left to right, the relation between the random potential in the channel of a MOSFET (assumed n -type) and the exponential tail in the density-of-states (DOS). Fig.1(a) shows a TEM picture of an older imec technology node with $\text{SiO}_2/\text{HfO}_2/\text{TiN}$ gate stack [21]. Fig.1(b) shows the blurring of the conduction-band edge $E_c(x)$ along a segment of the channel between x and $x + \Delta x$.

Following [22], the random potential in the channel is characterized by a Gaussian distribution. It is indeed reasonable to assume a Gaussian distribution since, according to the

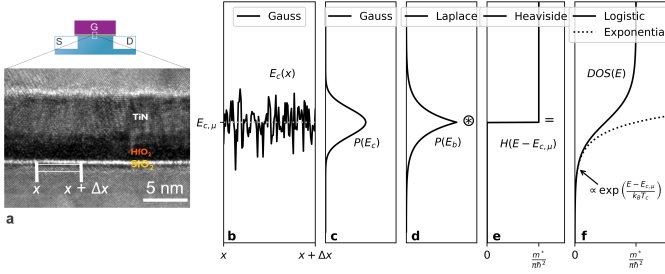


Fig. 1. a) TEM picture of a mature imec technology node [21], b) Electrostatic potential fluctuations near the channel/oxide interface, c) Gaussian distributed depths of the potential wells [22]. d) Including the binding energy in the quantum picture gives a Laplace distribution of $P(E_b)$ [22]. e)-f) Convolution (\otimes) of $P(E_b)$ with the sharp-edged 2-D DOS leads to a logistic/Fermi-like DOS function with an exponential tail.

central limit theorem, the aggregate of a large number of independent random variables still has a normal distribution even if the variables are not normally distributed. The Gaussian distribution of the depths of the local potential wells in $E_c(x)$,

$$P(E_c) \propto \exp\left(\frac{-(E_c - E_{c,\mu})^2}{2\sigma^2}\right) \quad (3)$$

is centered around the average $E_{c,\mu}$ with a standard deviation of σ [Fig. 1(c)]. To obtain the smeared-out DOS with band tailing, the probability distribution must be convolved with the sharp-edged DOS (see entry ‘‘H’’ in Table I), that is,

$$\begin{aligned} DOS(E) &= DOS_H \otimes P(E_c) \quad (4) \\ &= \int_{-\infty}^E DOS_H(E - E_c) \cdot P(E_c) \cdot dE_c \quad (5) \end{aligned}$$

where H stands for the Heaviside step function and \otimes stands for the convolution operation.

However, this convolution with a Gaussian distribution does not give rise to an exponential tail immediately. The resulting DOS would have an error function shape with tail $\propto \exp(-x^2)$ (see entry ‘‘G’’ in Table I). The exponential $DOS(E)$ arises out of the quantum picture, where the binding energies of the local potential wells in $E_c(x)$ are taken into account. Bacalis *et al.* found an approximately linear relation between the binding energy (E_b) and the square of the depth of the potential well for different types of wells: $|E_b - E_{c,\mu}| \simeq A \cdot (E_c - E_{c,\mu})^2 - B$ [22]. Inserting this expression in (3), we obtain a Laplace distribution for the binding energies

$$P(E_b) \propto \exp\left(\frac{-|E_b - E_{c,\mu}|}{k_B T_c}\right), \quad (6)$$

shown in Fig.1(d), where $k_B T_c = 2A\sigma^2$. The convolution of the sharp DOS, shown in Fig.1(e), with (6) gives a logistic- or Fermi-like distribution plotted in Fig. 1(f). The dashed line shows the exponential behavior below $E_{c,\mu}$, which is often referred to as a ‘‘band tail’’. Note, in the semi-classical picture (i.e., no binding energies considered, hence no panel d in Fig.1), ‘‘G’’ would be obtained. The Gaussian tail gives a steeper subthreshold slope as shown in Fig. 2(a), due to a less fat tail since $\propto \exp(-x^2)$ goes faster to zero than $\exp(-x)$. Fig. 2(b) also checks that, for current values in subthreshold ($\approx 10^{-8}$ A), it is sufficient to take into account the exponential

TABLE I
BAND-TAIL SHAPES

Symbol	DOS shape	DOS expression $x = (E - E_{c,\mu}) / k_B T_c$
H	Standard (sharp, no band tail)	$\frac{m^*}{\pi \hbar^2} \cdot H(x)$
G	Normal (Gauss)	$\frac{m^*}{\pi \hbar^2} \cdot 0.5 \cdot [\text{erf}(x) + 1]$
F	Logistic (Fermi)	$\frac{m^*}{\pi \hbar^2} \cdot [1 + \exp(-x)]^{-1}$
E	Exponential (subthreshold approx.)	$\frac{m^*}{\pi \hbar^2} \cdot \exp(x) \cdot H(-x)$

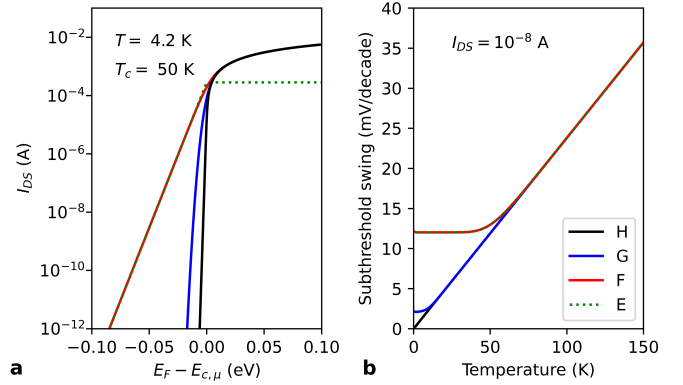


Fig. 2. For I_{DS} in subthreshold ($\approx 10^{-8}$ A), the SS obtained for a Fermi-like DOS (F : band tail + band) using numerical integration, falls on top of that for an exponential DOS (E , band tail only). Therefore, including only the exponential DOS, is a sufficiently accurate assumption for our present purposes of deriving a closed-form expression for SS .

tail of the DOS only, without the band states. This allows to derive a closed-form model for SS in the rest of the paper.

B. Subthreshold Swing Derivation

The subthreshold swing is defined as

$$SS \triangleq \frac{\partial V_{GS}}{\partial \log_{10}(I_{DS})} = \frac{I_{DS}}{\frac{\partial I_{DS}}{\partial V_{GS}}} \cdot \ln(10), \quad (7)$$

where I_{DS} is the drain-source current in subthreshold and V_{GS} is the gate-to-source voltage. The current flowing below $E_{c,\mu}$ would be accurately described by percolation theory [23]. The carriers percolate through the rugged potential landscape in Fig. 1(b). The band tail captures only the average effect of the potential fluctuations on the carriers traveling in a long channel. For short channels, tunneling and hopping currents need to be taken into account using the appropriate quantum formalism, see [24]. To obtain an expression for I_{DS} in subthreshold, we approximate this carrier flow with drift-diffusion transport in first order. We also adopt the gradual-channel and depletion approximations for obtaining the surface electric field from the 1-D MOS Poisson equation.

The mobile sheet charge density is then given by

$$Q_i \approx -(m - 1) \cdot C_{ox} \int_0^{\psi_s} \frac{n(\psi)}{N_A} \cdot d\psi \quad (8)$$

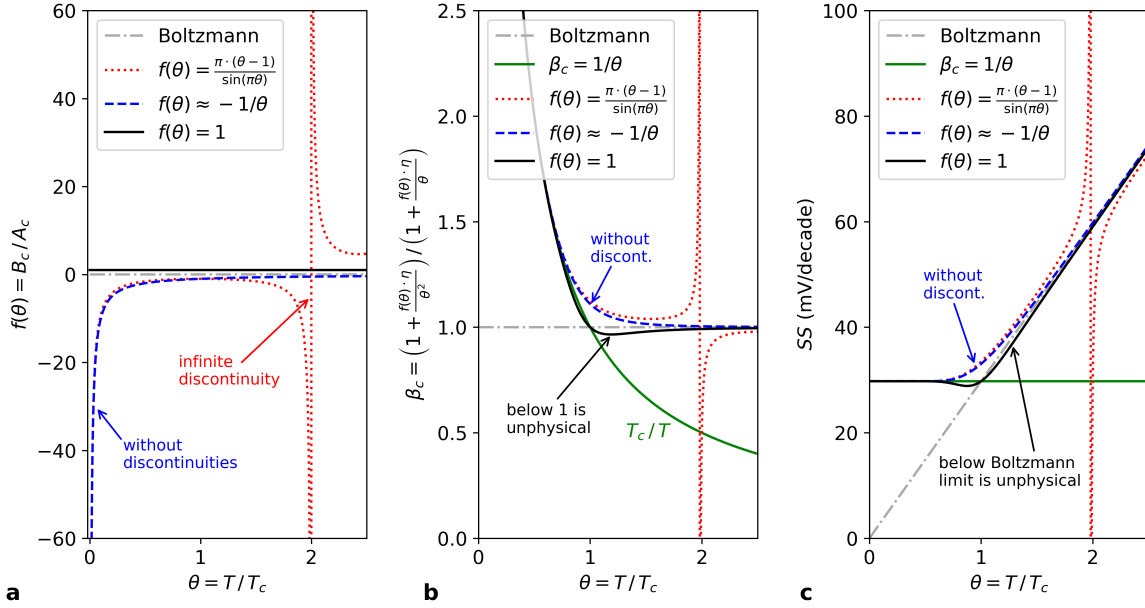


Fig. 3. (a) Function $f(\theta)$ from (14) and approximations. The infinite discontinuities arise from the analytical solution of the Fermi-Dirac integral with exponential DOS. (b) The fraction β_c from (13) for different approximations of $f(\theta)$. (c) $f(\theta) = 1$ is a too simplistic approximation which leads to unphysical behavior in SS around the transition temperature ($\theta = 1$). The green lines in (b) and (c) indicate the low-temperature asymptote. The model shown with the blue dashed line will be used further in the rest of the paper.

where C_{ox} is the gate-oxide capacitance, ψ_s is the surface potential, and N_A the doping concentration [25]. Recall that the Fermi-Dirac integral with exponential-tail DOS is

$$n = \int_{-\infty}^{E_c} DOS_E \left(\frac{E - E_c}{k_B T_c} \right) \cdot f_D(E) \cdot dE, \quad (9)$$

where $f_D(E)$ is the Fermi-Dirac distribution function and E_c is now the conduction-band edge at which the tail transitions into the band. This integral is exactly expressible as a Gauss hypergeometric (GH) function. Using mathematical formulas from Gradshteyn and Ryzhik for this special function [26], it is possible to derive a Boltzmann-like relation, which is valid in subthreshold. It features a sum of two exponentials: [27]

$$n(\psi) = N_c \cdot A_c \cdot \exp\left(\frac{\psi - \Phi_{F,n} - 0.5 \cdot E_g}{U_T}\right) + N_c \cdot B_c \cdot \exp\left(\frac{\psi - \Phi_{F,n} - 0.5 \cdot E_g}{U_{T,c}}\right), \quad (10)$$

where N_c is an effective DOS, $U_T \triangleq k_B T/q$ is the thermal voltage, $U_{T,c} \triangleq k_B T_c/q$ is the ‘‘band-tail thermal voltage’’, $q \cdot \psi = E_c^o - E_c$ is the electrostatic potential, $q \cdot \Phi_{F,n} = E_c^o - E_{F,n} - 0.5 \cdot E_g$ is the quasi-Fermi potential of the electrons, E_F is the Fermi level, and E_c^o is the reference energy. The temperature-dependent coefficients in (10) are given by

$$\begin{cases} A_c = \theta/(\theta - 1), \\ B_c = \pi\theta/\sin(\pi\theta), \end{cases} \quad (11)$$

where $\theta \triangleq T/T_c$ is the operating temperature normalized to the critical temperature. The coefficients A_c and B_c will be important to obtain a well-behaved expression for SS over T . The discontinuities of A_c and B_c at integer values of θ (multiples of T_c) do not necessarily point to a limitation

in the derivation or in the physical assumptions. They can arise from the Gamma functions which are encountered in the mathematics of the Fermi-Dirac integrals with an exponential DOS [27]. The expression for I_{DS} is further derived in the Appendix, see (22)-(28). Differentiating (28) to V_{GS} and plugging the result back into the definition of SS (7), gives

$$SS = m \cdot \left(\frac{k_B T}{q} \right) \cdot \ln(10) \cdot \beta_c, \quad (12)$$

where

$$\beta_c = \frac{1 + f \cdot \eta/\theta^2}{1 + f \cdot \eta/\theta}, \quad (13)$$

is a new multiplicative factor that contains the influence of the band tail. Recall that $\theta = T/T_c$ is the normalized temperature, and we have also defined the following functions

$$f = \frac{B_c}{A_c} = \frac{\pi \cdot (\theta - 1)}{\sin(\pi\theta)}, \quad (14)$$

$$\eta = r \cdot e^{\frac{-V_{GS}}{m \cdot U_T} \cdot (1-\theta)}, \quad (15)$$

and

$$r = \left(1 - e^{\frac{-V_{DS}}{U_{T,c}}} \right) / \left(1 - e^{\frac{-V_{DS}}{U_T}} \right). \quad (16)$$

Figs. 3(a)-(c) plot $f(\theta)$, $\beta_c(\theta, \eta)$, and SS versus θ , respectively. At $\theta = 2$, one of the infinite discontinuities appears, which arise at multiples of θ due to the sin-function in the denominator of $f(\theta)$. We aim to overcome these discontinuities noting that η goes fast to zero above T_c , therefore $f(\theta)$ is only important at low temperatures in the expression of β_c . The low-temperature asymptote [$\sin(\pi\theta) \approx \pi\theta$] gives $f(\theta) \approx -1/\theta$, and therefore β_c simplifies to

$$\beta_c \approx \frac{1 - \eta/\theta^3}{1 - \eta/\theta^2}, \quad (17)$$

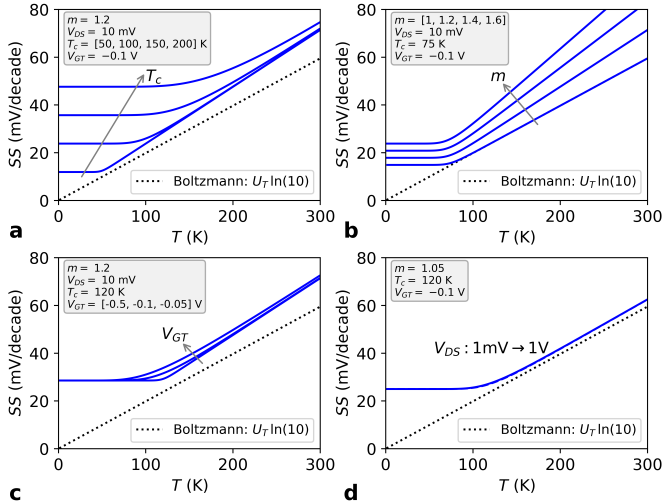


Fig. 4. Sensitivity analysis using (12) combined with (15), (16), and (17): (a) Impact of increasing band-tail width $\propto T_c$, (b) Impact of increasing slope factor m , (c) The gate voltage has some impact on the transition between the two limits, and (d) No significant impact seen from the V_{DS} dependence.

which does no longer give rise to infinite discontinuities at multiples of θ as shown with the dashed blue line in Fig.3(b). Fig.3(b) also shows that β_c has the elusive $1/\theta = T_c/T$ asymptote at low temperatures that we have been searching for [green solid line]. This $1/T$ dependence has been postulated in early hypotheses but was not derived there [17], [18]. It emerges from the I_{DS} factor instead of the slope factor. If the standard Boltzmann limit of SS , without β_c , is still used at cryogenic temperatures, an apparent $1/T$ -dependence in m will be extracted from the experimental SS data [20]. This can lead to unrealistic predictions of the interface-state density ($m \propto N_{it}$) [28], and thus β_c (or an equivalent expression) is best included. Parallels can be drawn between (12) and the empirical models which insert an effective slope-factor [17], [18] or an effective temperature [16] inside the Boltzmann limit, by defining $m_{\text{eff}} = m \cdot \beta_c$ or $T_{\text{eff}} = T \cdot \beta_c$ in (12).

Note that A_c and B_c in (10) were important to obtain a well-behaved transition around T_c . Assuming [$A_c = B_c = 1$ and thus $f(\theta) = 1$], which corresponds to a standard Boltzmann relation for the band carriers, plus assuming a step-like Fermi function in the band tail, gives rise to an unphysical $SS(T)$ behavior dropping below Boltzmann's thermal limit around $\theta = 1$, as shown with the black solid line in Fig. 3(c).

III. MODEL EXPLORATION, VERIFICATION, AND EXPERIMENTAL VALIDATION

A. Sensitivity of the Physical Model Parameters

In this section, we use the full expression, i.e., (12) combined with (15), (16), and (17), to explore the sensitivity to the physical model parameters m , T_c , V_{GT} , and V_{DS} . Fig. 4(a) shows that increasing T_c raises up the low- T plateau, which is in line with the literature [8]–[10]. This allows to extract the band-tail decay ($W_{t,c} = k_B T_c$) from transport measurements at cryogenic temperatures. Fig. 4(b) shows the impact of a larger slope factor due to bad gate control. The influence of m on SS is more pronounced in the high- T limit.

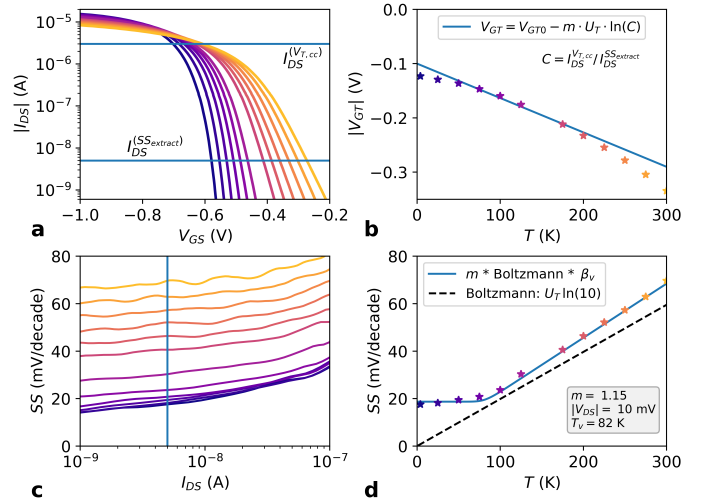


Fig. 5. Subthreshold swing for PMOS $W/L = 10 \mu\text{m}/1 \mu\text{m}$ from a 28-nm bulk CMOS process. (a) Transfer characteristics for $V_{DS} = 10 \text{ mV}$. (b) Difference between extracted gate voltage and threshold voltage at the two indicated current values. (c) Experimental SS data. (d) SS model fit.

Fig. 4(c) shows a smoother transition of SS around T_c for smaller $|V_{GT}|$ (V_G closer to V_T and E_F closer to the band edge scanning a greater portion of the band tail). Thus V_{GT} gives a (partial) physical explanation for the smoothing parameters α and D_0 introduced in the empirical closed-form expressions [(7), [10]] and [(9), [16]], respectively. V_{GT} is linked to the I_{DS} value at which SS is extracted from measurements ($I_{DS}^{SS, \text{extract}}$). This will be used as part of the parameter extraction procedure for long devices in Section III-B. Fig. 4(d) shows the model for two different high and low V_{DS} (1 mV up to 1 V). No noticeable difference is obtained.

B. Extraction Procedure for Long Devices

A long $p\text{MOS}$ ($W/L = 10 \mu\text{m}/1 \mu\text{m}$), a long $n\text{MOS}$ ($3 \mu\text{m}/1 \mu\text{m}$) and a short $n\text{MOS}$ ($3 \mu\text{m}/30 \text{ nm}$) from a commercial 28-nm bulk CMOS technology were measured down to 4.2 K using a Lakeshore cryogenic probe station. The transfer characteristics were recorded using a Keysight B1500A semiconductor device analyzer at $V_{DS} = 10 \text{ mV}$.

Fig. 5(a) shows the measured $I_D - V_G$ curves for the long $p\text{MOS}$. The horizontal line indicates the current at which the SS and V_T are extracted (constant current method), respectively $I_{DS}^{(SS, \text{extract})} = 5 \times 10^{-9} \text{ A}$ and $I_{DS}^{(V_T, cc)} = 3 \times 10^{-6} \text{ A}$. Using interpolation, the $V_G(T)$ and $V_T(T)$ data points are obtained from the experimental data at these two I_{DS} values. Their difference V_{GT} is then plotted in Fig. 5(b) [markers]. We observe that V_{GT} has an approximately linear trend vs. temperature. A first-order model can be obtained for the V_{GT} -dependence in the model by writing two expressions for I_{DS} in the high-temperature limit ($T > T_c$) [first term in (28)]:

$$I_{DS}^{(V_T^{cc})} = K \cdot U_T^2 \cdot \left(1 - e^{-\frac{V_{DS}}{U_T}}\right) \quad (18)$$

$$I_{DS}^{(SS, \text{extract})} = K \cdot U_T^2 \cdot e^{\frac{V_{GT}}{m U_T}} \left(1 - e^{-\frac{V_{DS}}{U_T}}\right) \quad (19)$$

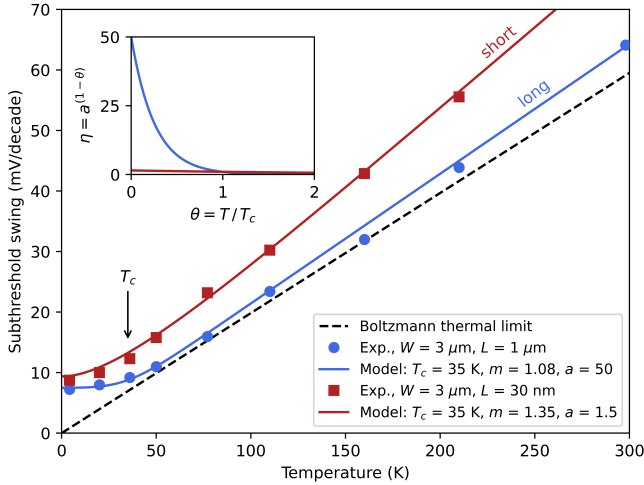


Fig. 6. Model (21) is calibrated to the n MOS devices with long and short channels. If the gate length shortens, the plateau at very low temperatures lies higher because the slope factor is larger for short devices (worse gate control). We also see a smoother roll-off around the transition region for shorter devices. Inset shows the simplified η -function from (15), where a is a smoothing parameter; a comes partly from the V_{GT} dependence derived in the long-channel model [see Fig.4(c)] but here it is given some more freedom.

Dividing both expressions, we obtain

$$V_{GT} = V_{GT0} - m \cdot U_T \cdot \ln \left(\frac{I_{DS}^{V_{T,cc}}}{I_{DS}^{SS,extract}} \right) \quad (20)$$

where the added V_{GT0} is the linearly extrapolated V_{GT} at ≈ 0 K. The constant current method is useful here to extract V_T because the K (including material parameters μ and C_{ox}) cancels out. Fig. 5(c) plots the experimental SS versus I_{DS} . The temperature trend of SS is extracted at $I_{DS} = 5 \times 10^{-9}$ A and shown in Fig. 5(d). The model is then fitted to the data according to the following procedure. First, the linear V_{GT} model is fit to the experimental data in Fig. 5(b), using m , V_{GT0} , and the two known current values. The slope factor m is then further adjusted by looking at the high-temperature slope of $SS(T)$ in Fig. 5(d). Finally, T_c (or T_v for p MOS) is determined from the low-temperature plateau of $SS(T)$.

C. Simplified Formula for Long and Short Devices

As explained in Sec.II-B, the model is built on long-channel assumptions. Here we give the model some additional freedom in the transition region around T_c to be able to fit both long and short devices. Replacing $e^{\frac{-V_{GT}}{m \cdot U_T}}$ in (15) with a parameter $a > 1$, (and $r \rightarrow 1$, i.e., neglect V_{DS} in the model), we obtain

$$SS = m \cdot \left[\frac{1 - a^{1-\theta}/\theta^3}{1 - a^{1-\theta}/\theta^2} \right] \cdot \frac{k_B T}{q} \cdot \ln(10), \quad (21)$$

which is shown in Fig. 6. For long (short) devices the transition below T_c to the low-temperature plateau is sharper (smoother), therefore a is set to a larger (smaller) value. This causes $a^{1-\theta}/\theta^3$ and $a^{1-\theta}/\theta^2$ to dominate faster (slower) over 1 in the numerator and denominator of (21), hence SS levels off faster (slower) to $m \cdot [1/\theta] \cdot (k_B T/q) \cdot \ln(10) = m \cdot (k_B T_c/q) \cdot \ln(10)$.

IV. CONCLUSION

A closed-form and physics-based expression is derived for the saturation of SS in MOSFETs based on band-tail physics. Exponential band tails can arise from Gaussian-distributed potential well depths in the channel if their binding energies are taken into account. The obtained SS model showed that the Boltzmann thermal limit becomes multiplied with a new factor that depends on temperature and voltage. In the low-temperature limit, this new factor revealed the long-sought $1/T$ -dependence, which has often been postulated in previous literature. We started from a more general set of Boltzmann relations which was essential to arrive at a well-behaved transition around T_c . The gate-voltage dependence could partly explain the smoother roll-off around the transition temperature. The drain voltage dependence showed little impact. In the future, band-tail extraction can become a powerful tool to gauge interface quality in MOS structures for cryogenic computing.

APPENDIX

Similarly, for the hole density, we have

$$p = N_v \cdot A_v \cdot \exp \left(\frac{-\psi + \Phi_{F,p} - 0.5 \cdot E_g}{U_T} \right) + N_v \cdot B_v \cdot \exp \left(\frac{-\psi + \Phi_{F,p} - 0.5 \cdot E_g}{U_{T,v}} \right), \quad (22)$$

where A and B remain the same as in (11), except that $\theta = T/T_v$, with $k_B T_v$ the extension of the valence-band tail.

Since the valence-band tail will have little to no influence on the SS for an n MOSFET, we make a symmetric band-tail approximation ($T_c \approx T_v$; $N_c \approx N_v$) and assume that $A_v = B_v = 1$. Furthermore, the effects of dopant freeze-out and dopant ionization can be ignored in computing the SS . Therefore the charge-neutrality in the p -type bulk of the MOSFET ($\psi = 0$) is simply $p \approx N_A$, which yields two useful formulas at low and high temperatures, respectively:

$$\exp \left(\frac{-0.5 \cdot E_g}{U_{T,c}} \right) = \frac{N_A}{N_c} \cdot \exp \left(\frac{-\Phi_F}{U_{T,c}} \right), \quad (23)$$

$$\exp \left(\frac{-0.5 \cdot E_g}{U_T} \right) = \frac{N_A}{N_c} \cdot \exp \left(\frac{-\Phi_F}{U_T} \right). \quad (24)$$

where $\Phi_{F,p} \triangleq \Phi_F = \Phi_{F,n} - V$, and V is the channel voltage or difference in quasi-Fermi potentials. Inserting (23) and (24) into (10), we obtain the following expression

$$\frac{n(\psi)}{N_A} = A_c \cdot \exp \left(\frac{\psi - 2\Phi_F - V}{U_T} \right) + B_c \cdot \exp \left(\frac{\psi - 2\Phi_F - V}{U_{T,c}} \right). \quad (25)$$

Combining (25) with (8), integrating, and applying the subthreshold relation, $V_{GS} = m \cdot \psi_s$, and the threshold-voltage definition, $V_T \triangleq m \cdot 2\Phi_F$, we obtain the sheet-charge density,

$$-Q_i = (m-1) \cdot C_{ox} \cdot U_T \cdot A_c \cdot e^{\frac{V_{GT}-mV}{m \cdot U_T}} + (m-1) \cdot C_{ox} \cdot U_{T,c} \cdot B_c \cdot e^{\frac{V_{GT}-mV}{m \cdot U_{T,c}}}, \quad (26)$$

where $V_{GT} = V_{GS} - V_T < 0$ in subthreshold. The exponential with the largest denominator ($m \cdot U_T$ or $m \cdot U_{T,c}$) will

dominate. At high T ($U_T \gg U_{T,c}$ or $\theta \gg 1$), this is the first exponential, and $A_c \rightarrow 1$, which recovers the standard Q_i at room temperature [25]. At low T ($U_T \ll U_{T,c}$ or $\theta \ll 1$), the second exponential dominates, and $B_c \rightarrow 1$ [$\sin(x) \approx x$ for small x]. The drift-diffusion current in the MOSFET is [25]

$$I_{DS} = \mu \cdot \frac{W}{L} \int_0^{V_{DS}} -Q_i(V) \cdot dV, \quad (27)$$

where μ is the channel mobility, W and L the width and length of the transistor, and V_{DS} the drain-to-source voltage. Integrating (27) with Q_i from (26), we find a voltage- and T -dependent expression for the subthreshold current:

$$I_{DS} = K \cdot U_T^2 \cdot A_c \cdot e^{\frac{V_{GT}}{m \cdot U_T}} \left(1 - e^{-\frac{V_{DS}}{U_T}} \right) + K \cdot U_{T,c}^2 \cdot B_c \cdot e^{\frac{V_{GT}}{m \cdot U_{T,c}}} \left(1 - e^{-\frac{V_{DS}}{U_{T,c}}} \right), \quad (28)$$

where $K = \mu \cdot \frac{W}{L} \cdot (m - 1) \cdot C_{ox}$.

REFERENCES

- [1] M. Gonzalez-Zalba, S. de Franceschi, E. Charbon, T. Meunier, M. Vinet, and A. Dzurak, "Scaling silicon-based quantum computing using CMOS technology," *Nature Electronics*, pp. 1–13, 2021, doi: [10.1038/s41928-021-00681](https://doi.org/10.1038/s41928-021-00681).
- [2] F. Jazaeri, A. Beckers, A. Tajalli, and J.-M. Sallese, "A Review on Quantum Computing: From Qubits to Front-end Electronics and Cryogenic MOSFET Physics," *IEEE*, Jun. 2019, pp. 15–25, doi: [10.23919/MIXDES.2019.8787164](https://doi.org/10.23919/MIXDES.2019.8787164).
- [3] F. Sebastiano, J. van Dijk, P. 't Hart, B. Patra, J. van Staveren, X. Xue, C. Almudever, G. Scappucci, M. Veldhorst, L. Vandersypen, A. Vladimirescu, S. Pellerano, M. Babaie, and E. Charbon, "Cryo-CMOS Interfaces for Large-Scale Quantum Computers," in *2020 IEEE International Electron Devices Meeting (IEDM)*, 2020, pp. 25.2.1–25.2.4, doi: [10.1109/IEDM13553.2020.9372075](https://doi.org/10.1109/IEDM13553.2020.9372075).
- [4] F. Tavernier, A. Gatti, and C. Barretto, "Chip Design for Future Gravitational Wave Detectors," *IEEE*, Dec. 2020, pp. 25.4.1–25.4.4, doi: [10.1109/IEDM13553.2020.9372071](https://doi.org/10.1109/IEDM13553.2020.9372071).
- [5] D. Braga, S. Li, and F. Fahim, "Cryogenic Electronics Development for High-Energy Physics: An Overview of Design Considerations, Benefits, and Unique Challenges," *IEEE Solid-State Circuits Magazine*, vol. 13, no. 2, pp. 36–45, 2021. [Online]. Available: <https://ieeexplore.ieee.org/document/9467069/>
- [6] H. L. Chiang, T. C. Chen, J. F. Wang, S. Mukhopadhyay, W. K. Lee, C. L. Chen, W. S. Khwa, B. Pulicherla, P. J. Liao, K. W. Su, K. F. Yu, T. Wang, H. S. P. Wong, C. H. Diaz, and J. Cai, "Cold CMOS as a Power-Performance-Reliability Booster for Advanced FinFETs," in *2020 IEEE Symposium on VLSI Technology*. Honolulu, HI, USA: IEEE, Jun. 2020, pp. 1–2. [Online]. Available: <https://ieeexplore.ieee.org/document/9265065/>
- [7] D. Prasad, M. Vangala, M. Bhargava, A. Beckers, A. Grill, D. Tierno, K. Nathella, T. Achuthan, D. Pietromonaco, J. Myers, M. Walker, B. Parvais, and B. Cline, "Cryo-Computing for Infrastructure Applications: A Technology-to-Microarchitecture Co-optimization Study," in *2022 International Electron Devices Meeting (IEDM)*, doi: [10.1109/IEDM45625.2022.10019436](https://doi.org/10.1109/IEDM45625.2022.10019436).
- [8] H. Bohuslavskiy, A. G. M. Jansen, S. Barraud, V. Barral, M. Cassé, L. Le Guevel, X. Jehl, L. Hutin, B. Bertrand, G. Billiot, G. Pillonnet, F. Arnaud, P. Galy, S. De Franceschi, M. Vinet, and M. Sanquer, "Cryogenic Subthreshold Swing Saturation in FD-SOI MOSFETs Described With Band Broadening," *IEEE Electron Device Letters*, vol. 40, no. 5, pp. 784–787, May 2019, doi: [10.1109/LED.2019.2903111](https://doi.org/10.1109/LED.2019.2903111).
- [9] A. Beckers, F. Jazaeri, and C. Enz, "Theoretical Limit of Low Temperature Subthreshold Swing in Field-Effect Transistors," *IEEE Electron Device Letters*, vol. 41, no. 2, pp. 276–279, Feb. 2020, doi: [10.1109/LED.2019.2963379](https://doi.org/10.1109/LED.2019.2963379).
- [10] G. Ghibaudo, M. Aouad, M. Cassé, S. Martinie, T. Poiroux, and F. Balestra, "On the modelling of temperature dependence of subthreshold swing in MOSFETs down to cryogenic temperature," *Solid-State Electronics*, vol. 170, p. 107820, Aug. 2020, doi: [10.1016/j.sse.2020.107820](https://doi.org/10.1016/j.sse.2020.107820).
- [11] R. M. Jock, S. Shankar, A. M. Tyryshkin, J. He, K. Eng, K. D. Childs, L. A. Tracy, M. P. Lilly, M. S. Carroll, and S. A. Lyon, "Probing band-tail states in silicon metal-oxide-semiconductor heterostructures with electron spin resonance," *Applied Physics Letters*, vol. 100, no. 2, p. 023503, Jan. 2012, doi: [10.1063/1.3675862](https://doi.org/10.1063/1.3675862).
- [12] B. Richstein, Y. Han, Q. Zhao, L. Hellmich, J. Klos, S. Scholz, L. R. Schreiber, and J. Knoch, "Interface Engineering for Steep Slope Cryogenic MOSFETs," *IEEE Electron Device Letters*, vol. 43, no. 12, pp. 2149–2152, Dec. 2022. [Online]. Available: <https://ieeexplore.ieee.org/document/9930783/>
- [13] Y. Han, J. Sun, B. Richstein, F. Allibert, I. Radu, J.-H. Bae, D. Grützmacher, J. Knoch, and Q.-T. Zhao, "Steep Switching Si Nanowire p-FETs With Dopant Segregated Silicide Source/Drain at Cryogenic Temperature," *IEEE Electron Device Letters*, vol. 43, no. 8, pp. 1187–1190, 2022, doi: [10.1109/LED.2022.3185781](https://doi.org/10.1109/LED.2022.3185781).
- [14] D. Frank, R. Dennard, E. Nowak, P. Solomon, Y. Taur, and H.-S. P. Wong, "Device scaling limits of Si MOSFETs and their application dependencies," *Proceedings of the IEEE*, vol. 89, 2001, doi: [10.1109/5.915374](https://doi.org/10.1109/5.915374).
- [15] K.-H. Kao, T. R. Wu, H.-L. Chen, W.-J. Lee, N.-Y. Chen, W. C.-Y. Ma, C.-J. Su, and Y.-J. Lee, "Subthreshold Swing Saturation of Nanoscale MOSFETs Due to Source-to-Drain Tunneling at Cryogenic Temperatures," *IEEE Electron Device Letters*, vol. 41, no. 9, pp. 1296–1299, 2020, doi: [10.1109/LED.2020.3012033](https://doi.org/10.1109/LED.2020.3012033).
- [16] G. Pahwa, P. Kushwaha, A. Dasgupta, S. Salahuddin, and C. Hu, "Compact Modeling of Temperature Effects in FDSOI and FinFET Devices Down to Cryogenic Temperatures," *IEEE Transactions on Electron Devices*, vol. 68, no. 9, pp. 4223–4230, Sep. 2021, doi: [10.1109/TED.2021.3097971](https://doi.org/10.1109/TED.2021.3097971).
- [17] S. Tewksbury, "Attojoule MOSFET logic devices using low voltage swings and low temperature," *Solid-State Electronics*, vol. 28, no. 3, pp. 255–276, Mar. 1985, doi: [10.1016/0038-1101\(85\)90006-1](https://doi.org/10.1016/0038-1101(85)90006-1).
- [18] A. Akturk, M. Holloway, S. Potbhare, D. Gundlach, B. Li, N. Goldsman, M. Peckerar, and K. P. Cheung, "Compact and Distributed Modeling of Cryogenic Bulk MOSFET Operation," *IEEE Transactions on Electron Devices*, vol. 57, no. 6, pp. 1334–1342, Jun. 2010, doi: [10.1109/TED.2010.2046458](https://doi.org/10.1109/TED.2010.2046458).
- [19] C. Enz, A. Beckers, and F. Jazaeri, "Cryo-CMOS Compact Modeling," *IEEE IEDM Conference*, Dec. 2020, pp. 25.3.1–25.3.4, doi: [10.1109/IEDM13553.2020.9371894](https://doi.org/10.1109/IEDM13553.2020.9371894).
- [20] A. Beckers, F. Jazaeri, and C. Enz, "Characterization and Modeling of 28-nm Bulk CMOS Technology Down to 4.2 K," *IEEE Journal of the Electron Devices Society*, vol. 6, pp. 1007–1018, 2018, doi: [10.1109/JEDS.2018.2817458](https://doi.org/10.1109/JEDS.2018.2817458).
- [21] L.-A. Ragnarsson, Z. Li, J. Tseng, T. Schram, E. Rohr, M. J. Cho, T. Kauerauf, T. Conard, Y. Okuno, B. Parvais, P. Absil, S. Biesemans, and T. Y. Hoffmann, "Ultra low-EOT (5 Å) gate-first and gate-last high performance CMOS achieved by gate-electrode optimization," in *2009 IEEE International Electron Devices Meeting (IEDM)*, Dec. 2009, pp. 1–4, doi: [10.1109/IEDM.2009.5424254](https://doi.org/10.1109/IEDM.2009.5424254).
- [22] N. Bacalis, E. N. Economou, and M. H. Cohen, "Simple derivation of exponential tails in the density of states," *Physical Review B*, vol. 37, no. 5, pp. 2714–2717, Feb. 1988. [Online]. Available: <https://link.aps.org/doi/10.1103/PhysRevB.37.2714>
- [23] E. Catapano, M. Cassé, and G. Ghibaudo, "Cryogenic MOSFET Subthreshold Current: From Resistive Networks to Percolation Transport in 1-D Systems," *IEEE Transactions on Electron Devices*, pp. 1–6, 2023, doi: [10.1109/TED.2023.3283941](https://doi.org/10.1109/TED.2023.3283941).
- [24] H.-C. Han, H.-L. Chiang, I. P. Radu, and C. Enz, "Analytical Modeling of Source-to-Drain Tunneling Current Down to Cryogenic Temperatures," *IEEE Electron Device Letters*, vol. 44, no. 5, pp. 717–720, 2023, doi: [10.1109/LED.2023.3254592](https://doi.org/10.1109/LED.2023.3254592).
- [25] Y. Taur and T. H. Ning, *Fundamentals of Modern VLSI Devices*. Cambridge University Press, 2021.
- [26] I. S. Gradshteyn and D. Zwillinger, *Table of Integrals, Series, and Products*, 8th ed. Boston: Elsevier, Academic Press, 2015.
- [27] A. Beckers, D. Beckers, F. Jazaeri, B. Parvais, and C. Enz, "Generalized Boltzmann relations in semiconductors including band tails," *Journal of Applied Physics*, vol. 129, no. 4, p. 045701, Jan. 2021, doi: [10.1063/5.0037432](https://doi.org/10.1063/5.0037432).
- [28] P. Galy, J. Camirand Lemyre, P. Lemieux, F. Arnaud, D. Drouin, and M. Pioro-Ladriere, "Cryogenic Temperature Characterization of a 28-nm FD-SOI Dedicated Structure for Advanced CMOS and Quantum Technologies Co-Integration," *IEEE Journal of the Electron Devices Society*, vol. 6, pp. 594–600, 2018, doi: [10.1109/JEDS.2018.2828465](https://doi.org/10.1109/JEDS.2018.2828465).